# Identification of rare HIV-1–infected patients with extreme CD4+ T cell decline despite ART-mediated viral suppression

**Andrea Lisco,[1] Chun-Shu Wong,[1] Silvia Lucena Lage,[1] Itzchak Levy,[2] Jason Brophy,[3] Jeffrey Lennox,[4] Maura Manion,[1] Megan V. Anderson,[1] Yolanda Mejia,[1] Christopher Grivas,[1] Harry Mystakelis,[1] Peter D. Burbelo,[5] Ainhoa Perez-Diez,[1] Adam Rupert,[6] Craig A. Martens,[7] Sarah L. Anzick,[7] Caryn Morse,[1] Shanna Chan,[8] Claire Deleage,[9] and Irini Sereti[1]**

[1]Laboratory of Immunoregulation, HIV Pathogenesis Section, National Institute of Allergy and Infectious Diseases (NIAID), NIH, Bethesda, Maryland, USA. [2]Sheba Medical Center, Tel Hashomer and the Sackler Medical School, Tel Aviv, Israel. [3]Children's Hospital of Eastern Ontario, Ottawa, Canada. [4]Grady Memorial Hospital, Emory University, Atlanta, Georgia, USA. [5]Dental Clinical Research Core, National Institute of Dental and Craniofacial Research, NIH, Bethesda, Maryland, USA. [6]AIDS Monitoring Laboratory, Leidos Biomedical Research, Frederick, Maryland, USA. [7]Rocky Mountain Laboratory, Genomics Unit, NIAID, NIH, Hamilton, Montana, USA. [8]Winnipeg Regional Health Authority, Manitoba, Canada. [9]Tissue Analysis Core, AIDS and Cancer Virus Program, Leidos Biomedical Research Inc., Frederick National Laboratory for Cancer Research, Frederick, Maryland, USA.

**BACKGROUND.** The goal of antiretroviral therapy (ART) is to suppress HIV-1 replication and reconstitute CD4+ T cells. Here, we report on HIV-infected individuals who had a paradoxical decline in CD4+ T cells despite ART-mediated suppression of plasma HIV-1 load (pVL). We defined such an immunological outcome as extreme immune decline (EXID).

**METHODS.** EXID's clinical and immunological characteristics were compared to immunological responders (IRs), immunological nonresponders (INRs), healthy controls (HCs), and idiopathic CD4+ lymphopenia (ICL) patients. T cell immunophenotyping and assembly/activation of inflammasomes were evaluated by flow cytometry. PBMC transcriptome analysis and genetic screening for pathogenic variants were performed. Levels of cytokines/chemokines were measured by electrochemiluminescence. Luciferase immunoprecipitation system and NK-mediated antibody-dependent cellular cytotoxicity (ADCC) assays were used to identify anti-lymphocyte autoantibodies.

**RESULTS.** EXIDs were infected with non-B HIV-1 subtypes and after 192 weeks of consistent ART-mediated pVL suppression had a median CD4+ decrease of 157 cells/μl, compared with CD4+ increases of 193 cells/μl and 427 cells/μl in INR and IR, respectively. EXID had reduced naive CD4+ T cells, but similar proportions of cycling CD4+ T cells and HLA-DR+CD38+CD8+ T cells compared with IR and INR. Levels of inflammatory cytokines were also similar in EXID and INR, but the IL-7 axis was profoundly perturbed compared with HC, IR, INR, and ICL. Genes involved in T cell and monocyte/macrophage function, autophagy, and cell migration were differentially expressed in EXID. Two of the 5 EXIDs had autoantibodies causing ADCC, while 2 different EXIDs had an increased inflammasome/caspase-1 activation despite consistently ART-suppressed pVL.

**CONCLUSIONS.** EXID is a distinct immunological outcome compared with previously described INR. Anti–CD4+ T cell autoantibodies and aberrant inflammasome/caspase-1 activation despite suppressed HIV-1 viremia are among the mechanisms responsible for EXID.

**Conflict of interest:** Jeffrey Lennox reports grants from ViiV Healthcare and personal fees from Gilead.



**Submitted:** January 3, 2019
**Accepted:** March 12, 2019
**Published:** April 18, 2019.

**Reference information:** *JCI Insight*. 2019;4(8):e127113. https://doi.org/10.1172/jci.insight.127113.

## Introduction

The goal of antiretroviral therapy (ART) is the suppression of HIV-1 replication and the ensuing reconstitution of CD4+ T cells. The improvement in morbidity and mortality associated with adequate CD4+ T cell reconstitution with ART has dramatically changed the natural history of HIV-1 infection. Nonetheless, a

considerable proportion of ART-treated individuals can only achieve a modest increase of $CD4^+$ T cells despite suppression of HIV-1 replication. These subjects are defined immunological nonresponders (INRs) and have a significantly higher mortality compared with immunological responders (IRs) (1–3). Although demographic (older age, male gender) and immunological variables (low nadir CD4, immune activation, lymphoid tissue fibrosis, and impaired homeostatic signaling) have been associated with a blunted immunological response to ART, the mechanisms underlying such phenomena remain elusive and therefore no adjunctive therapy improving $CD4^+$ T cell reconstitution is currently available (4, 5).

Here, we report on HIV-1–infected individuals who, despite consistent ART-mediated suppression of HIV-1 replication, developed a paradoxical decline in $CD4^+$ T cells. We present the epidemiological and immunological findings of such immunological outcome and propose what we believe are novel mechanisms associated with this extreme immune decline (EXID) in ART-treated subjects.

## Results

*Immunological response to ART*. Five subjects were referred to the NIH Clinical Center for declining $CD4^+$ T cells despite consistent suppression of plasma HIV-1 load (pVL) on different ART regimens and extensive work-up ruling out any concomitant malignancy. The demographic, clinical, and immunological characteristics of these subjects are summarized in Table 1 and supplemental material. The median age at time of enrollment was 25 years (range 13–49) and all subjects were infected with non-B HIV-1 subtypes. The median $CD4^+$ T cell count before ART was 179 cells/μl (IQR 67–414), but after 192 weeks of ART, despite consistent suppression of pVL on different regimens, the median $CD4^+$ T cells decreased to 36 cells/μl (IQR 17–60) (Figure 1). This paradoxical decline of $CD4^+$ T cells despite consistent ART-mediated pVL suppression was profoundly different from the immunological responses in ART-naive subjects with nadir $CD4^+$ less than 100 cells/μl on ART for 192 weeks. The median difference in $CD4^+$ T cells between baseline and week 192 of ART in EXID was –157 cells/μl (IQR –376 to –40) compared with an increase of 193 cells/μl (IQR 161–300) and 427 cells/μl (IQR 300–568) in INR ($n$ = 15) and IR ($n$ = 8), respectively (Figure 1B).

We defined this unexpected immunological outcome as extreme immune decline (EXID), because not only was it in sharp contrast with IR, it was even inferior to INR.

*Distinct T cell immunophenotype and cytokine/chemokine profile in EXID*. Because the proportions of $CD4^+$ T cell maturation subsets and of activated T cells have been proposed as correlates of poor $CD4^+$ T cell recovery (4), we evaluated the distribution of different T cell subsets in healthy controls (HC, $n$ = 13) as well as in IR, INR, and EXID after 96 weeks of ART.

The median proportion of naive $CD4^+$ T cells was not significantly different between IR and HC (43% and 43%, respectively), while it was significantly lower in EXID compared with IR and HC (4% compared with 43%, Supplemental Figure 1 and Supplemental Figure 2; supplemental material available online with this article; https://doi.org/10.1172/jci.insight.127113DS1). Similarly, the median proportion of central memory $CD4^+$ T cells, which was not different between IR, INR, and HC (43%, 45%, and 50%, respectively), was significantly reduced in EXID compared with HC and INR (15%). The lower proportion of naive and central memory $CD4^+$ T cells observed in EXID was associated with a relative increase in the effector memory $CD4^+$ T cells (66%) compared with HC and IR (5% and 8% respectively, Supplemental Table 1 and Supplemental Figure 2). EXID was also associated with a lower proportion of naive and central memory and relative increase in effector and effector memory $CD8^+$ T cells compared with HC (Supplemental Table 1 and Supplemental Figure 3), but the differences in the proportions of these $CD8^+$ T cell subsets between EXID and IR or INR were not statistically significant.

An increased proportion of cycling $CD4^+$ T cells and activated T cells has been associated with INR (4) and, in fact, we found that the proportion of cycling memory $CD4^+$ T cells ($CD45RO^+Ki67^+$) and activated ($HLA\text{-}DR^+CD38^+$) $CD4^+$ and $CD8^+$ T cells was significantly increased in INR compared with HC (Figure 2 and Supplemental Table 1). In contrast, EXID was not associated with a higher proportion of cycling memory $CD4^+$ T cells or activated $CD8^+$ T cells compared with HC, IR, or INR (Figure 2 and Supplemental Table 1), but rather with a marked increase in the frequency of $PD1^+$ memory $CD4^+$ T cells (59% vs. 8%) and of activated ($HLA\text{-}DR^+CD38^+$) $CD4^+$ T cells (7% vs. 0.6%) compared with HC (Figure 2 and Supplemental Table 1).

To further characterize the immunological milieu in EXID, we compared the plasma/serum levels of 21 cytokines/chemokines in EXID, HC, IR, INR, and patients with idiopathic CD4 lymphopenia (ICL, $n$ = 11), a heterogeneous clinical syndrome with low $CD4^+$ T cells (median 27 cells/μl [IQR 2–217]) in the absence of HIV-1 infection or any other known primary or acquired immunodeficiency (6). The cyto-

**Table 1. General characteristics of the subjects with extreme immune decline (EXID)**

| | EXID 1 | EXID 2 | EXID 3[A] | EXID 4 | EXID 5 | EXID (all) median |
|---|---|---|---|---|---|---|
| **Age at enrollment** | 49 | 18 | 13 | 25 | 40 | **25** |
| **Gender** | F | M | M | M | F | **60% M/40% F** |
| **HIV-1 subtype** | CRF BC | C | C | CRF AG | D | **na** |
| **Country** | Zambia | Congo | Congo | Israel | Zambia | **na** |
| **ART (wks)** | 536 | 593 | 357 | 159 | 254 | **357** |
| **ART** | TFV/FTC/EFV | AZT/3TC/NLF | AZT/3TC/rLPV | TFV/FTC/RPV | TFV/FTC/EFV | **3 regimens** |
| | ABC/3TC/rATZ | D4T/3TC/rLPV | TFV/FTC/cEVG | TFV/FTC/rLPV | | |
| | TFV/FTC/rATZ | ABC/3TC/rLPV | TFV/FTC/rDRV | AZT/3TC/rLPV | | |
| | EFV/RAL | ABC/EFV/rATZ/RAL | | | | |
| **CD4 before ART** | 102 | 315 | 179 | 587 | 22 | **179** |
| **CD4 week 192 ART** | 36 | 52 | 26 | 68 | 9 | **36** |
| **HLA** | A*30, 4301 | A*68 | A*29, 68 | A*03, 24 | A*02, 68 | |
| | B*18, 57 | B*13, 18 | B*07:05:01G | B*07, 18 | B*42, 01 | |
| | CW*07, 07 | CW*04, 06 | | CW*07, 15 | CW*17 | |
| | DRB1*0804, 11 | DRB1*11, 13 | | DRB1*12, 14 | DRB1*08, 13 | |
| **Peak HIV-1 pVL (copies/ml)** | >100,000 | 82,000 | 13,163 | 660 | >100,000 | **82,000** |

[A]Perinatally infected subject. ABC, abacavir; AZT, zidovudine; cEVG, cobicistat/elvitegravir; D4T, stavudine; EFV, efavirenz; FTC, emtricitabine; FTV, ; NLF, nelfinavir; RAL, raltegravir; rATZ, ritonavir/atazanavir; rDRV, ritonavir/darunavir; rLPV, ritonavir/loprinavir; RPV, rilpivirine; 3TC, lamivudine; TFV, tenofovir.

kine profile of EXID was distinct, with lower concentrations of TNF-α compared with INR, and IL-12 compared with HC. The most apparent difference in EXID, however, was that the levels of IL-7 were significantly higher compared with HC and IR (Figure 3 and Supplemental Table 2). We documented a negative correlation between the serum IL-7 levels and the $CD4^+$ T cell counts among HIV-1–infected subjects (Spearman's $\rho$ –0.53 [CI 95% –0.76 to –0.17], $P < 0.004$, Supplemental Figure 4) and IR, INR, and EXID segregated as 3 distinct clusters in relation to these 2 variables.

*Impaired IL-7/IL-7 receptor axis in EXID*. To investigate the integrity of the IL-7 signaling axis, we compared the expression of the IL-7 receptor α-chain (CD127) and STAT5 phosphorylation status in response to IL-7 between the 3 EXID patients for which sufficient material was available (EXID2, -3, and -4) and other patients' groups.

The proportion of $CD127^+$ effector memory $CD4^+$ T cells was 55% in EXID, 94% in HC, 82% in IR, and 71% in INR (Figure 4A and Supplemental Table 1). Similar differences in CD127 expression were also observed in the central memory $CD4^+$ T cell subset (Figure 4B and Supplemental Table 1), but not in naive $CD4^+$ T cells of the 4 groups. A significantly lower expression of CD127 was observed in $CD8^+$ T cells from EXID compared with HC, IR, and INR (Supplemental Table 2). The transcriptional effects of IL-7 are mediated by STAT5 phosphorylation (p-STAT5) and its subsequent nuclear translocation; stimulation with 10 ng of IL-7 resulted in a median 3.8-fold (IQR 3.5–4.5) increase in p-STAT5 mean fluorescence intensity (MFI) in $CD4^+$ T cells from HC. Although INR and IR were both associated with a larger increase in p-STAT5 MFI in response to IL-7 compared with HC (INR 5.8 [IQR 5.5–6.8]; IR 6.9 [IQR 5.7–7.2]), EXID had a blunted p-STAT5 induction of 3.3-fold (IQR 2.4–3.4), significantly lower compared with HC, INR, and IR (Figure 4, C and D). Similar differences were also noted with stimulation at lower concentrations of IL-7 (1 ng/ml, Figure 4D).

*EXID is associated with a distinct transcriptional profile*. We next compared the transcriptional profile of peripheral blood mononuclear cells (PBMCs) from EXID patients with those of HC, ICL (median $CD4^+$ T cells 115 cells/μl), and paired HIV/AIDS untreated subjects before ART (median HIV-1 pVL 196,418 copies/ml; $CD4^+$ T cells 45 cells/μl) and after 96 weeks of ART (median HIV-1 pVL < 40 copies/ml; $CD4^+$ T cells 317 cells/μl).

No differences in the number of differentially expressed genes (DEGs) were found between ART-treated subjects and HC; in contrast, a considerable number of genes were differentially regulated in EXID compared with HC, HIV/AIDS untreated, and ART-treated IR ($n = 138$, $n = 269$, $n = 313$, respectively), while a more limited group of genes distinguished ICL and EXID transcriptomes ($n = 24$, Figure 5, A and B, and Supplemental Table 3). The EXID transcriptome was distinct from HC, HIV/AIDS untreated, and ART-treated IR; hierarchical clustering of a group of 320 genes with functional roles in innate or adaptive

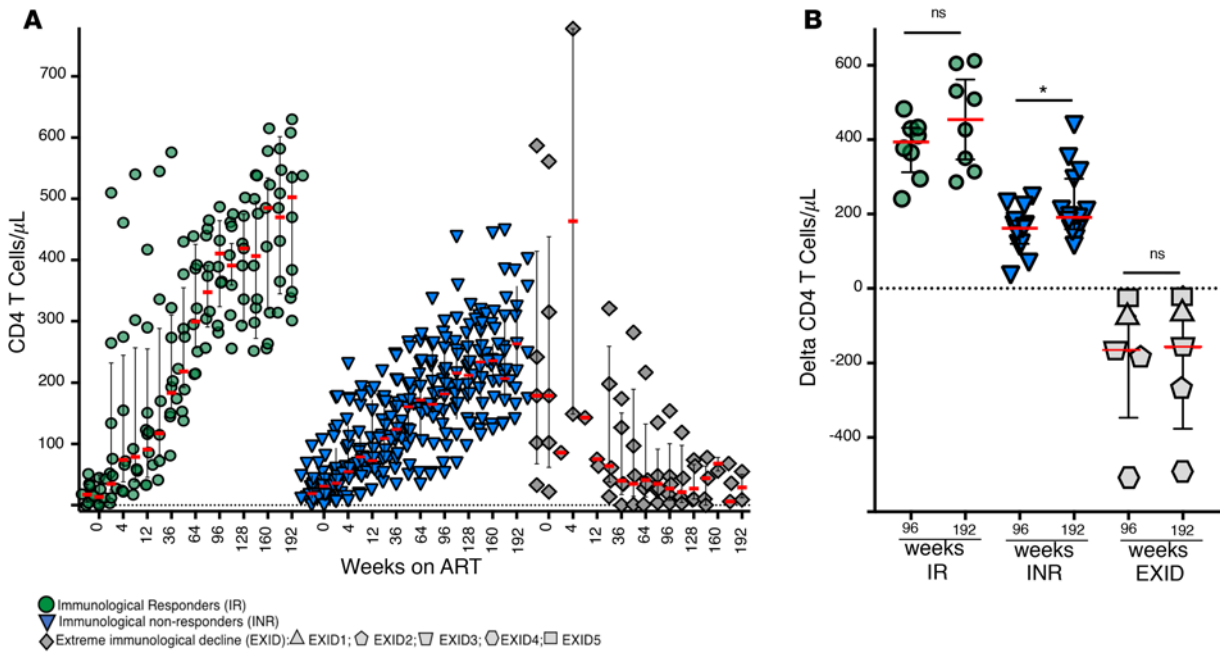


**Figure 1. CD4⁺ T cell trends after ART initiation.** (**A**) CD4⁺ T cell count in immunological responders (IRs), immunological nonresponders (INRs), and extreme immunological decline (EXID) after initiation of ART. The median (red bar), IQR (error bar), and each available CD4⁺ T cell count measurement (symbols) is presented at each time point for IR ($n$ = 8), INR ($n$ = 15), and EXID ($n$ = 5). (**B**) The median (red bar), IQR (error bar), and the difference in CD4⁺ T cell count between week 0 (ART initiation) and week 96 or week 192 (symbols) is presented for each IR ($n$ = 8), INR ($n$ = 15), and EXID ($n$ = 5) subject. Each EXID subject is identified by a different gray-filled shape. *$P \leq 0.05$ in the comparison indicated by the black horizontal line as determined by Mann-Whitney $U$ test; ns, nonsignificant difference.

immune responses revealed 3 clusters of genes, differentially regulated in EXID, HC, HIV/AIDS untreated, and ART-treated IR subjects (red, green, and blue clusters in Figure 5A and Supplemental Tables 4 and 5).

In addition, the list of the top best-scoring DEGs ($\log_2$ fold change [FC] ≥ 1.5 [18 genes] or ≤ –1.5 [20 genes], adjusted $P$ value ≤ 0.005; Figure 5C) in EXID compared with ART-treated IR subjects was enriched with genes involved in T cell function, TCR signaling, monocyte/macrophage function, autophagy, and cell migration (Supplemental Tables 4 and 5, and Supplemental Figure 5). The DEGs between EXID and ART-treated IR were different from the DEGs found between EXID and HIV/AIDS untreated; in fact, 118 and 61 genes were respectively downregulated or upregulated in EXID compared with HIV/AIDS untreated subjects but only 1 of these genes was among the DEGs between EXID with ART-treated IR (TNFAIP2; Figure 5, B and C, and Supplemental Figure 5). This analysis demonstrated that the transcriptome in EXID is different from both HIV/AIDS untreated subjects with severe CD4⁺ T cell depletion (median 45 cells/μl) as well as from paired ART-treated subjects with CD4⁺ T cell reconstitution (317 cells/μl). Such a distinct transcriptome characterized by the differential regulation of genes and pathways involved in T cell and macrophage/monocyte functions as well as autophagy and inflammation prompted additional genetic work-up to evaluate the presence of rare hypomorphic genetic variants in genes involved in the control of similar immunological functions.

*Genetic screening for variants associated with primary immunodeficiencies in EXID.* We performed targeted next-generation sequencing (NGS) on 3 of the 5 EXID subjects for which sufficient material was available. EXID2 had a heterozygous variant in the gene RTEL1 (regulator-of-telomeres elongation helicase-1, NM_016434-codon_1322G>A, protein_W441*, combined annotation-dependent depletion [CADD] score 36), introducing a premature stop codon possibly resulting in nonsense-mediated decay. EXID2 did not have laboratory or clinical findings consistent with autosomal dominant telomeropathies classically associated with pathogenic RTEL1 variants (dyskeratosis congenita, Online Mendelian Inheritance in Man [OMIM#615190] and pulmonary fibrosis and/or bone marrow failure [OMIM#616373]) (7), but had a significant reduction in telomere length (TL) in total naive T cells (median TL: 6.5 vs. 8.1 kilobases [kb] in control of same age [CSA], 1–10 percentile), memory T cells (median TL: 3.8 vs. 6.5 kb in CSA, <1 percentile), CD57⁺ lymphocytes (NK) (median TL: 3.5 vs. 6.8 kb in CSA, <1 percentile), but not in B cells (median TL: 7.6 vs. 8.3 kb in CSA, 10–90 percentile)

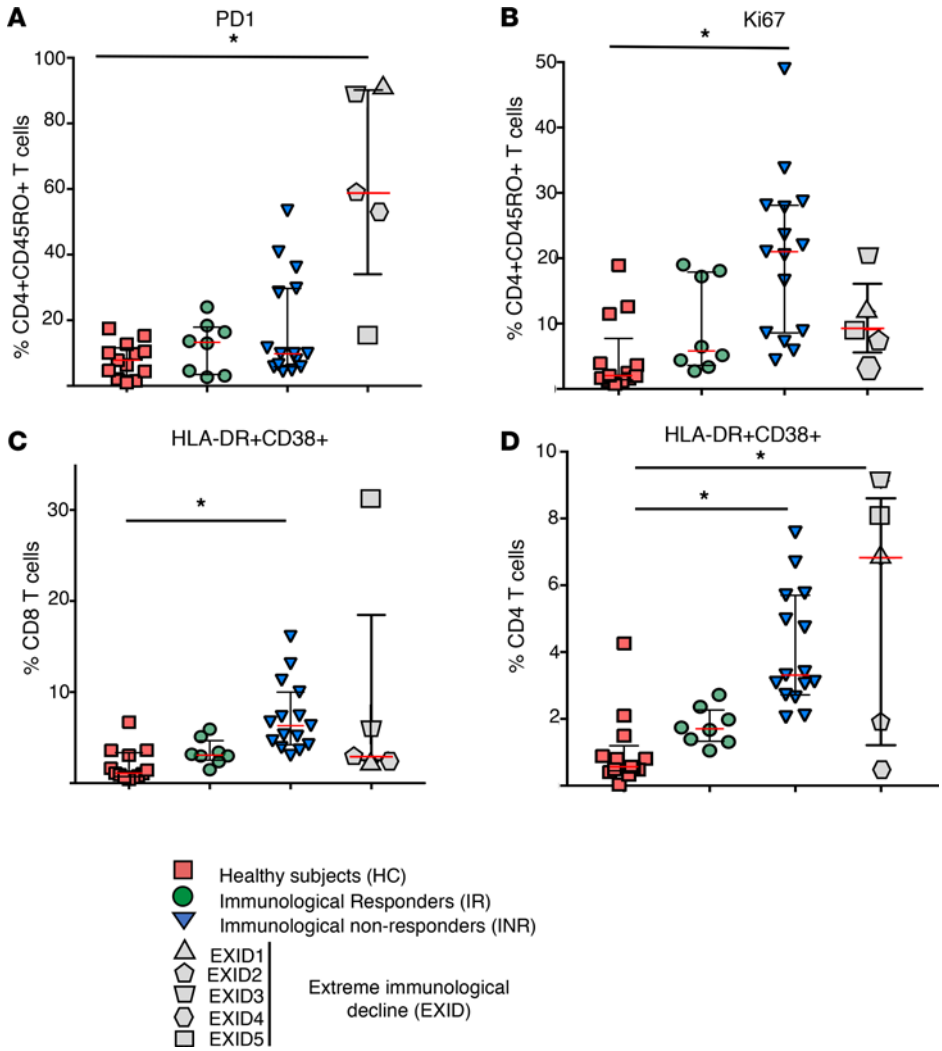


**Figure 2. T cell immunophenotyping in healthy controls, IR, INR, and EXID.** (**A**) Proportion of PD1-expressing memory CD4$^+$ T cells (CD45RO$^+$). (**B**) Proportion of Ki67-expressing memory CD4$^+$ T cells (CD45RO$^+$). (**C**) Proportion of HLA-DR$^+$CD38$^+$ CD8$^+$ T cells. (**D**) Proportion of HLA-DR$^+$CD38$^+$ CD4$^+$ T cells. The median (red bar), IQR (error bar), and each subject (symbols) is presented for healthy controls (HC) ($n$ = 13), IR ($n$ = 8), INR ($n$ = 15), EXID ($n$ = 5). Each EXID subject is identified by a different gray-filled shape. *$P \leq 0.05$ in the comparison indicated by the black horizontal line as determined by Kruskal-Wallis test followed by Dunn's post-hoc test.

(Supplemental Figure 6). Genetic screening in EXID3 did not reveal obvious causative variants but a heterozygous missense variant of unknown significance was identified in the gene ATG9A (autophagy-related protein 9A, NM_024085-codon_2473G>A, protein_E825K, CADD score 33) (8). In EXID4 we identified a heterozygous pathogenic variant in the gene MEFV (pyrin, NM_000243-codon2080A>G, protein_M694V, CADD score 0.01) associated with Mediterranean fever (9, 10) and a rare variant in the gene NLRP7 (NLR family pyrin domain–containing 7, NM_001127255-codon_2156C>T, protein_A719V, CADD score 15.89) (11).

*Anti-lymphocyte autoantibodies in EXID.* Because cytopenias are seen in autoimmune conditions and in primary immunodeficiencies (12, 13), we evaluated the presence of anti-lymphocyte autoantibodies possibly causing autoimmune destruction, impaired homeostatic expansion, or altered trafficking of CD4$^+$ T cells in EXID, IR, or INR. Luciferase immunoprecipitation system (LIPS) immunoassay did not identify autoantibodies against several T cell surface proteins (CD3δ, CD3ε, CD3γ, CD8α, CD8β, CD4, CTL4, CD127, IFN-γ receptor-1, and IL-2 receptor γ-chain) nor against Ro52/TRIM21, a common target of autoantibodies in several autoimmune diseases, in any of the subjects. As an alternative strategy, we developed an NK cell–mediated antibody-dependent cellular cytotoxicity (ADCC) assay to reveal autoantibodies against any other epitopes expressed on CD4$^+$ T cells. By this assay we found that CD4$^+$ T cells were

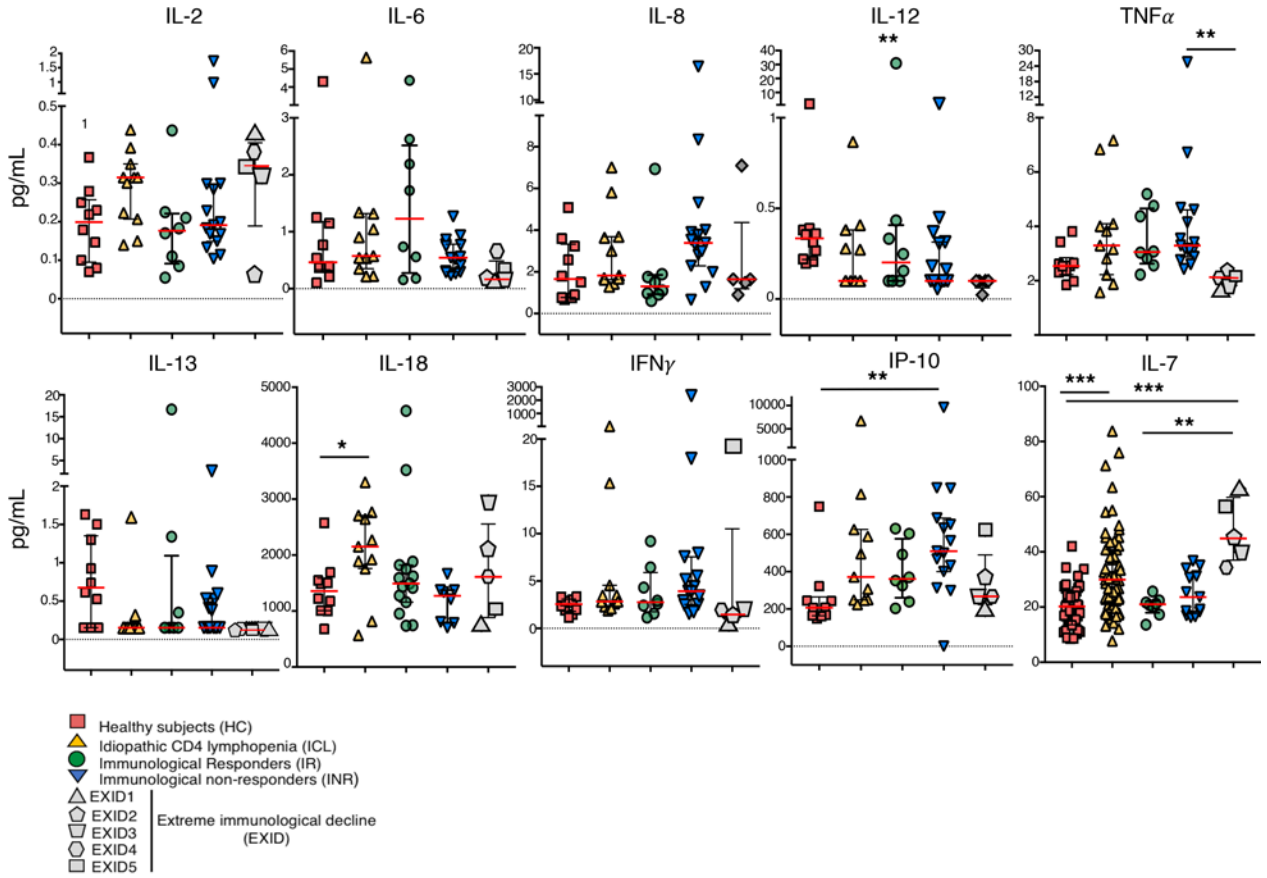


**Figure 3. Cytokine/chemokine levels in HC, IR, INR, and EXID and idiopathic CD4 lymphopenia.** The median (red bar), IQR (error bar), and each subject (symbols) is presented for HC ($n$ = 10), idiopathic CD4 lymphopenia (ICL) ($n$ = 11), IR ($n$ = 8), INR ($n$ = 15), and EXID ($n$ = 5). IL-7 levels were measured in serum for HC ($n$ = 39), IR ($n$ = 8), INR ($n$ = 13), EXID ($n$ = 5), and ICL ($n$ = 60). Each EXID subject is identified by a different gray-filled shape. *$P \le 0.05$, **$P \le 0.01$, ***$P \le 0.001$ in the comparison indicated by the black horizontal line as determined by Kruskal-Wallis test followed by Dunn's post-hoc test.

specifically depleted when incubated with plasma from EXID1 and EXID5 but not with PBS, HC, IR, or INR plasma, nor plasma of other EXID patients (Figure 6). NK-mediated ADCC of $CD4^+$ T cells was more evident at higher effector/target (E/T) ratios, reaching an average of 50% of target $CD4^+$ T cells at a 40:1 E/T ratio. In addition, $CD4^+$ T cell killing was not observed when EXID1 or EXID5 plasma was IgG depleted, while the IgG eluate was sufficient to provide $CD4^+$ T cell NK-mediated ADCC (Figure 6). The same subjects (EXID1 and EXID5) also had evidence of NK-mediated ADCC of $CD19^+$ B cells in plasma; such ADCC activity was abolished by IgG depletion of plasma but was not associated with a decrease in the number of CD19-expressing B cells in peripheral blood.

*Long-term follow-up of EXID subjects*. Long-term clinical and immunological follow-up was available for all EXID subjects. EXID2 and EXID3 did not have evidence of opportunistic infections, immune reconstitution, nor specific clinical events.

The $CD4^+$ T cells of EXID1 remained below the pre-ART level, 36 cells/μl (5%), with 1.25% naive after approximately 5 years of consistent suppression of HIV-1 pVL, but in the following 7 years progressively increased, reaching 607 cells/μl (19%), with 17% naive (Supplemental Figure 7). We evaluated the presence of NK-mediated ADCC in plasma samples collected before and after the $CD4^+$ T cell recovery (week 188 and week 551 after ART initiation, respectively). No NK-mediated ADCC $CD4^+$ T cell killing was found in the latter samples (Figure 6), supporting the causative role of such autoantibodies in hampering immune reconstitution.

EXID5's $CD4^+$ T cells, after approximately 226 weeks of ART, started to progressively increase (highest $CD4^+$ T cell counts: 119 cells/μl, 12% on week 249 after ART) (Supplemental Figure 7). Alongside such $CD4^+$ T cell reconstitution, EXID5 developed mental status decline with radiological evidence of basilar arteritis and cerebral ischemic lesions. A clinical diagnosis of CNS tuberculosis was formulated but the patient was lost to follow-up after initiation of antituberculous therapy.

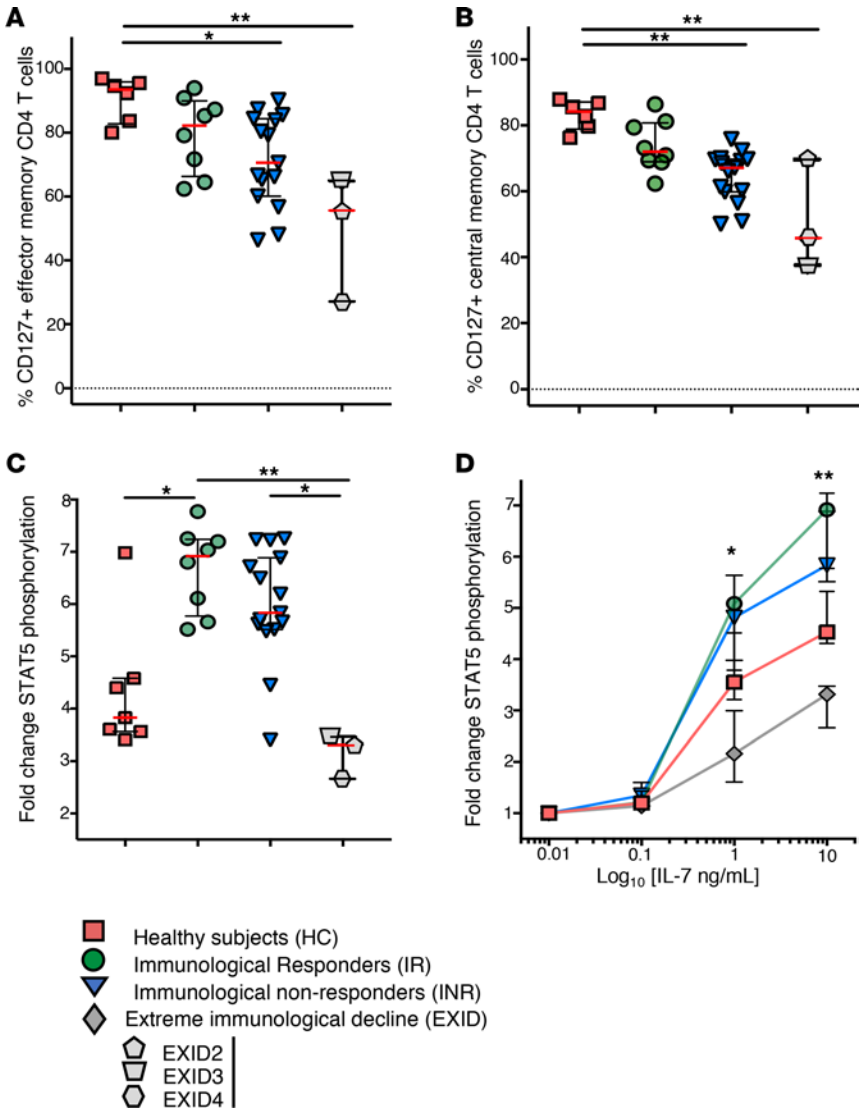


**Figure 4. IL-7 signaling axis in HC, IR, INR, and EXID.** (**A**) Proportion of CD127-expressing effector memory CD4$^+$ T cells (CD27$^-$CD45RO$^+$). (**B**) Proportion of CD127-expressing central memory CD4$^+$ T cells (CD27$^+$CD45RO$^+$). (**C**) Fold change in STAT5 phosphorylation upon IL-7 stimulation (10 nM). (**D**) Dose-response of STAT5 phosphorylation at different concentrations of IL-7. The median (red bar), IQR (error bar), and each subject (symbols) is presented for HC ($n$ = 6), IR ($n$ = 8), INR ($n$ = 15), and EXID ($n$ = 3). Each EXID subject is identified by a different gray-filled shape; sufficient material for the analysis was available from EXID2, -3, and -4. *$P \leq 0.05$, **$P \leq 0.01$ in the comparison indicated by the black horizontal line as determined by Kruskal-Wallis test followed by Dunn's post-hoc test.

EXID4 maintained stable CD4$^+$ T cells below the pre-ART level, 68 cells/μl (11%) with 4.3% naive (Supplemental Material Case Reports), despite 3 years of consistent suppression of HIV-1 pVL, but eventually developed right eye pain due to an infiltrating, hypermetabolic right orbital mass causing displacement of the right superior extraocular muscle and modeling of the superior right orbital bone as seen on MRI and PET-CT. A biopsy of the mass documented dense fibrosis and granulomas of epithelioid myeloid cells consistent with idiopathic orbital inflammation (IOI) (Supplemental Figure 8). This rare clinical entity has unknown etiology, but is associated with other inflammatory diseases and can cause a local infiltrating, destructive sclerosing process (14, 15). His inguinal lymph node histology and quantitative imaging documented a prominent IFN-α signature, increased collagen-1 deposition with accumulation of myeloid cells, and overall preserved CD4$^+$ T cell density in the follicular area and T cell zone compared with HC and paired HIV/AIDS untreated and ART-treated IR subjects (Supplemental Figures 8 and 9). Infliximab treatment, indicated in IOI (16), resulted in regression of the orbital

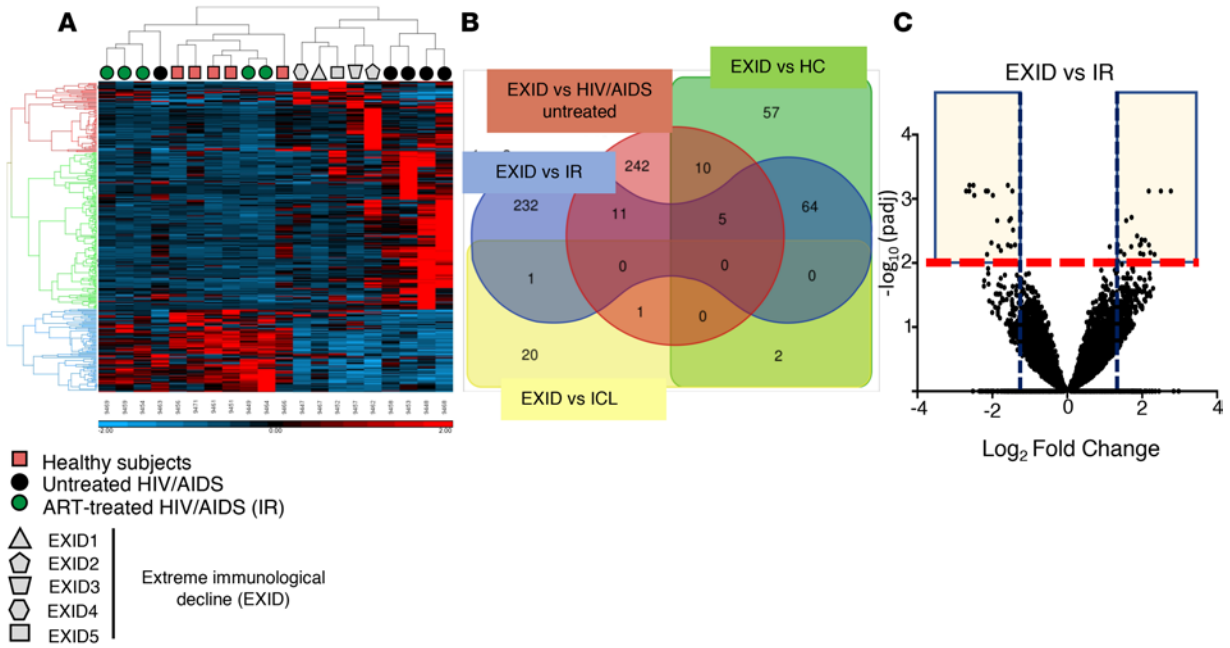


**Figure 5. Transcriptional profile of peripheral blood mononuclear cells from EXID, HC, and paired HIV/AIDS subjects before and after ART.** (**A**) Hierarchical clustering of 320 genes with functional role in innate or adaptive immune responses in HC ($n$ = 5), EXID ($n$ = 5), HIV/AIDS untreated ($n$ = 5), and ART-treated IR subjects ($n$ = 5). Each EXID subject is identified by a different gray-filled shape. (**B**) Edwards-Venn 4-set diagram depicting the number and the intersection of differentially regulated genes (DEGs) in 4 comparisons (EXID vs. HC [green], EXID vs. ICL [yellow], EXID vs. IR [blue], and EXID vs. HIV/AIDS untreated [red]). (**C**) Volcano plot of DEGs in EXID compared with ART-treated HIV/AIDS subjects. The shaded area identifies the top differentially downregulated ($\log_2$ fold change ≤ 1.5, 20 genes) or upregulated ($\log_2$ fold change ≤ 1.5, 18 genes) genes (listed in Supplemental Table 5).

mass, and was associated with a progressive recovery of CD4$^+$ T cells reaching 454 cells/μl (24%), with proportions of naive and effector memory CD4$^+$ T cells of 0.21% and 80.9%, respectively, after 12 months of infliximab (Supplemental Figures 8 and 9).

In the context of myeloid granulomas and an underlying inflammatory disorder possibly causing CD4$^+$ T cell pyroptosis (17, 18), we performed an analysis of inflammasome and caspase-1 activation in monocytes and T cells of EXID2 and EXID4 and found that monocytes had an increased number of apoptosis-associated speck-like protein containing a C-terminal caspase recruitment domain (ASC) colocalizing with caspase-1 compared with HC, IR, and INR (EXID2 124,852 cells/ml, EXID4 69,858 cells/ml, compared with 3096 cells/ml, 7710 cells/ml, and 6159 cells/ml, in HC, IR, and INR, respectively; Figure 7, A and B). CD4$^+$ T cells had a higher level of caspase-1 activation in EXID and INR compared with IR and HC (EXID2 7.3%, EXID4 2.8%, and INR 4.7%, compared with 2.5% and 1.9% in HC and IR, respectively); conversely, caspase-1 activation was negligible and not significantly different in CD8$^+$ T cells from HC, IR, INR, or EXID (Supplemental Figure 10).

## Discussion

Herein, we report, for the first time to our knowledge, on a paradoxical decline in CD4$^+$ T cells occurring after initiation of ART, which persisted despite consistent suppression of HIV pVL and changes in ART regimens. A comprehensive prospective clinical, immunological, and genetic characterization of these patients led to the identification of what we believe are novel mechanisms causing CD4$^+$ T cell depletion in ART-treated individuals, specifically autoimmunity and inflammasome/caspase-1 activation.

The hallmark of HIV/AIDS, in the context of uncontrolled HIV-1 viral replication, is the progressive depletion of CD4$^+$ T cells; direct viral cytopathic effects, apoptosis, pyroptosis, and immune-mediated lysis are among the mechanisms evoked to explain such depletion. Irrespective of the specific role of each of these mechanisms, ART-mediated suppression of HIV-1 replication results in reconstitution of CD4$^+$ T cells in all HIV-1–infected subjects. In fact, although the extent of immune reconstitution can vary, a decline of CD4$^+$ T cells on ART has never been described to the best of our knowledge, except as drug-related cytotoxicity of combined tenofovir-didanosine treatment (19).

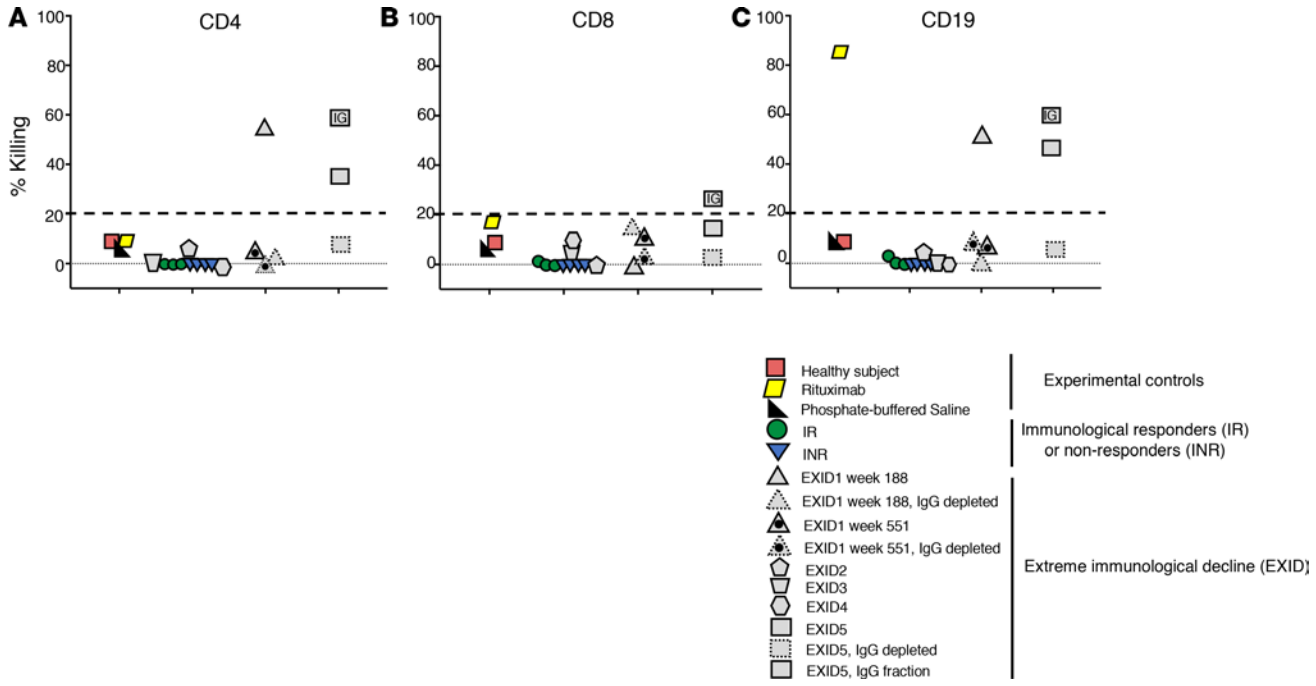


**Figure 6. NK cell–mediated antibody-dependent cellular cytotoxicity of EXID1 plasma.** Plotted is the percentage of killing (percentage difference in cell counts between untreated control and any experimental condition) of (**A**) $CD4^+$ T cells, (**B**) $CD8^+$ T cells, and (**C**) $CD19^+$ B cells incubated with PBS, rituximab, and plasma from a heathy subject, IR ($n$ = 3), INR ($n$ = 4), or EXID ($n$ = 5) at an effector/target ratio of 10:1 (PBS and rituximab) or 40:1 for all other experimental conditions. Each EXID subject is identified by a different gray-filled shape. Antibody-dependent cellular cytotoxicity (ADCC) activity was noted only in plasma of EXID1 and EXID5 for which additional experimental conditions were included.

Therefore, we identified an immunological outcome of ART, extreme immunological decline or EXID, in subjects infected with non-B HIV-1 subtypes, an observation suggesting a role for a specific combination of both host and viral factors in the pathogenesis of such rare and perplexing immunological outcome. EXID was not associated with previously described predictors of poor immune response, as it occurred in young individuals, with higher nadir $CD4^+$ and without any consistent increase in cycling $CD4^+$ T cells or activated $CD4^+$ or $CD8^+$ T cells. In fact, rather than an extreme form of INR, EXID appears distinct from INR, as it is characterized by the following: decline of $CD4^+$ T cell counts after initiation of ART, which remained consistently below the pre-ART level for at least 192 weeks despite constant suppression of pVL below the limit of detection; profound reduction of naive and relative expansion of effector memory $CD4^+$ T cells; distinct immunophenotypic (low Ki67, high PD-1) and plasma biomarker profile (low TNF and IL-12); and high serum IL-7 levels with downregulated IL-7 receptor expression and impaired STAT5 phosphorylation.

The perturbation in the IL-7 axis and the lack of adequate $CD4^+$ T cell expansion in response to increased IL-7 levels in EXID was not associated with an increase in inflammatory cytokines IL-6 and IL-1β, as proposed in INR (5), and appears to be more in line with those observed in ICL (20). It is conceivable that the blunted IL-7 axis can contribute to EXID, but it is also possible that it develops in response to a persistent compensatory mechanism that fails to achieve the homeostatic expansion of $CD4^+$ T cells because of additional mechanisms preventing adequate T cell reconstitution (i.e., antilymphocyte autoantibodies, aberrant inflammatory responses in genetically predisposed individuals).

The transcriptome analysis further documented a distinct transcriptional signature of EXID compared with paired viremic and ART-treated immunological responders characterized by different regulation of genes involved in T cell function, TCR signaling, monocyte/macrophage function, autophagy, and cell migration. In contrast, EXID's transcriptional signature was similar to that of subjects with ICL, suggesting some shared mechanisms responsible for the depletion of $CD4^+$ T cells possibly independent from HIV-1 direct cytopathic effects. Because EXID, ICL, and viremic HIV-1 individuals had a similar level of lymphopenia it is unlikely the changes in transcriptional signature between these groups were driven by the differences in relative numbers of $CD4^+$ T cell counts.

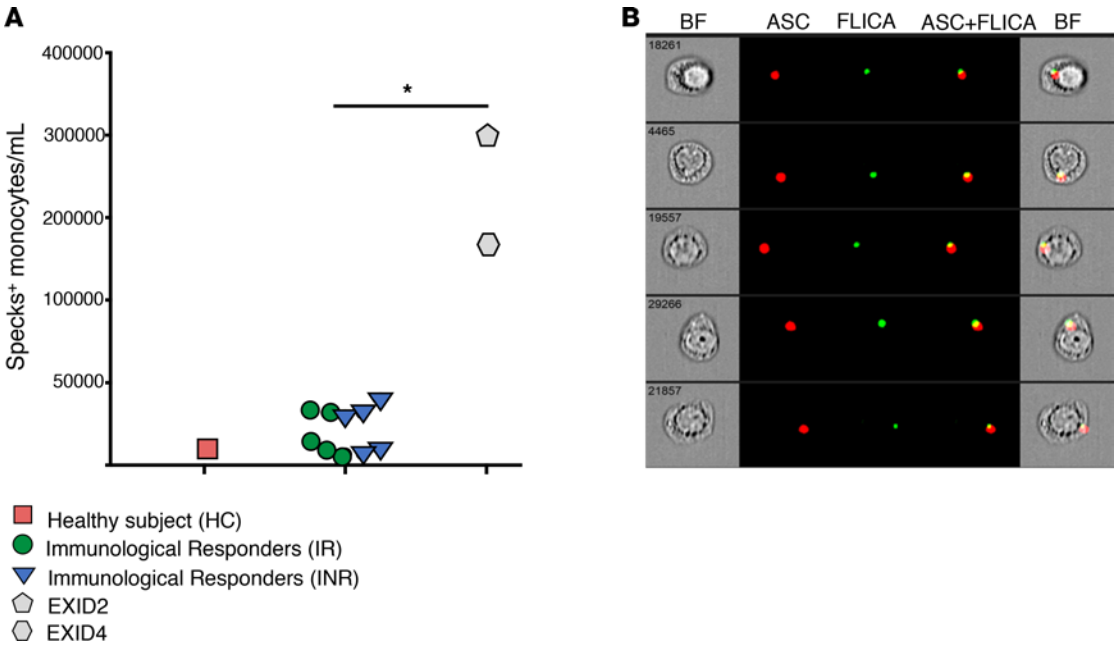


**Figure 7. Quantification of canonical inflammasome activation in CD14⁺ monocytes.** PBMCs from IR ($n$ = 5), INR ($n$ = 5), EXID2, EXID4, and a healthy subject were incubated with a fluorochrome-labeled inhibitor of caspase-1 (FAM-FLICA), stained for monocyte identification with antibodies against CD14 and the intracellular apoptosis-associated speck-like protein containing a C-terminal caspase recruitment domain (ASC), and evaluated by imaging flow cytometry. (**A**) The number of monocytes showing spontaneous ASC speck formation was quantified after application of the feature Area Threshold versus Modulation Morphology in the CD14-expressing monocyte gate, by ImageStream Data Exploration and Analysis Software (IDEAS 6.2.64.0, MilliporeSigma). Each EXID subject is identified by a different gray-filled shape. *$P \leq 0.05$ in the comparison indicated by the black horizontal line as determined by Mann-Whitney $U$ test. (**B**) Representative images showing colocalization of active caspase-1 with ASC specks were selected after Bright Detail Similarity was applied in the ASC speck gate. Images show, respectively: brightfield (BF), ASC and FLICA fluorescence followed by a composite image containing BF, and the fluorescence of ASC and FLICA merged.

The clinical follow-up provided important clues to the pathogenesis of EXID; a sustained recovery of CD4⁺ T cell counts was associated with the loss of anti-lymphocyte autoantibodies causing NK-mediated ADCC of CD4⁺ T cells in EXID1. An identical mechanism was also demonstrated in EXID5. The role of ADCC causing CD4⁺ T cell depletion has been previously documented in HIV-1–infected individuals (21–23) but its role in the pathogenesis of AIDS or immunological failure remains elusive. The evidence of recovery of CD4⁺ T cell counts after loss of such anti-lymphocyte autoantibodies has implication for the spontaneous reversibility of such a condition or for potential therapeutic interventions (i.e., rituximab or plasmapheresis). Importantly, the loss of anti-lymphocyte autoantibodies and consequent spontaneous recovery of CD4⁺ T cells occurred after more than 5 years of consistent suppression of pVL and in one case (EXID5) was also associated with symptoms and radiological findings consistent with immune reconstitution inflammatory syndrome that led to significant morbidity.

A spontaneous recovery of CD4⁺ T cell counts was not observed in any of the other 3 EXID subjects. However, the long-term follow-up of EXID4 revealed a different mechanism responsible for the CD4⁺ T cell decline; an orbital inflammatory disorder (IOI) prompted initiation of infliximab that resulted not only in the expected improvement of the orbital inflammatory mass but also in an unexpected reconstitution of CD4⁺ T cells. The CD4⁺ T cell recovery on infliximab, its pattern (lack of naive and expansion of effector memory CD4⁺ T cells), the increased inflammasome/caspase-1 activation along with lymph node fibrosis, and rare variants in genes controlling inflammasome/caspase-1 activation (NLRP7 and MEFV) (9–11), suggest a perturbed inflammatory response resulting in altered CD4⁺ T cell trafficking and homeostasis rather than autoimmune phenomena, which were in fact not documented in this subject. Interestingly, in a nonhuman primate model of acute SIV infection, adalimumab (TNF-α–blocking monoclonal antibody similar to infliximab) reduced lymph node fibrosis and preserved CD4⁺ T cells (24), while studies on TNF-α blockade in HIV-1–infected patients documented the safety of such intervention and an increase in CD4⁺ T cell counts in some case reports (25–28). EXID2 was found to have a remarkable inflammasome/caspase-1 activation along with severe decrease in TL, with an RTEL1 frameshift variant introducing an early stop codon. Such a

clinical scenario may resemble the recently reported novel quantitative and qualitative primary T cell immunodeficiency in which telomere shortening caused by specific genetic defects reaches a critical cellular threshold causing depletion of $CD4^+$ T cells from intrinsic and extrinsic apoptosis (29). It is conceivable that, as seen in this model, in EXID2, the telomere attrition caused by T cell replication in a perinatal HIV-1 infection with persistent vigorous inflammasome/caspase-1 activation could not be fully compensated for in the context of the frameshift variant in RTEL1 and reached a critical threshold in naive and memory T cells (7, 29, 30).

Despite the long-term follow-up and the prospective nature of our study, the small sample size and the variability in some immunological correlates imposed by the differences in the mechanism responsible for EXID limited our ability to generalize our findings. Nevertheless, we identified 2 mechanisms contributing to $CD4^+$ T cell depletion in subjects with suppressed HIV-1 replication, namely (a) autoimmune depletion of $CD4^+$ T cells, and (b) pyroptosis, impaired trafficking, and expansion of $CD4^+$ T cells in altered inflammasome/caspase-1 activation.

EXID is a rare immunological outcome of ART that may occur in patients with specific host and viral factors; EXID results in unique clinical challenges but can also reveal and help elucidate the specific mechanisms determining $CD4^+$ T cell depletion during uncontrolled HIV-1 replication from the ones limiting the degree of reconstitution of $CD4^+$ T cells on ART.

## Methods

*Study participants*. Patients referred to the NIH Clinical Center were enrolled in NIAID IRB–approved protocols after informed consent was obtained (NCT02147405, NCT00867269, NCT00001467, NCT00001281, NCT00286767, and NCT00789009). Written informed consent was provided for the patient's photo appearing in the supplemental material. IRs and INRs were defined as subjects with less than 100 $CD4^+$ T cells/μl on enrollment who achieved greater than or less than 270 $CD4^+$ T cells/μl after 96 weeks of ART, respectively. EXID was defined as a progressive and persistent decrease in $CD4^+$ T cell counts despite 192 weeks of ART in the absence of malignancy and regardless of pre-ART $CD4^+$ T cell counts. ICL is defined by less than 300 $CD4^+$ T cells/μl in the absence of HIV-1 infection or any other known primary or acquired immunodeficiency.

*Immunophenotyping and cytokine/chemokine quantification*. PBMCs were stained with fluorescently labeled antibodies against cell surface markers subsequently detected by flow cytometry. Sufficient material for the analysis of CD127 expression and STAT5 phosphorylation in response to IL-7 stimulation was available from EXID2, -3, and -4. Biomarkers were measured by electrochemiluminescence with a custom multiplex kit (Meso Scale Discovery).

*Transcriptome analysis and targeted NGS*. RNA was extracted from PBMCs of 5 EXID, 5 HC, 5 ICL, and 5 HIV/AIDS subjects prior to start and after 96 weeks of ART. The libraries were run on an Illumina HiSeq 2500 sequencer and reads were mapped to the human genome assembly NCBI-hg38 using Hisat2 (31). RNA sequence information reported in this study is deposited in NCBI's Gene Expression Omnibus (GEO GSE125223). The networks were generated through the use of IPA (QIAGEN Inc., https://www.qiagenbioinformatics.com/products/ingenuity-pathway-analysis).

Targeted NGS of exons and flanking regions of 318 genes causing primary immunodeficiencies was performed as previously described (32). Variants with a population frequency of less than 0.5% in different data sets (1000-Genomes, EXAC, NHLBI-6500, GnomAD) were scored using the CADD score.

*LIPS for measuring anti-lymphocyte antibodies and ADCC assays*. Autoantibodies against CD8α, CD8β, CD3δ, CD3ε, CD3γ, CD4, CTL4, IL-7 receptor, IFN-γ receptor-1, IL-2 receptor γ-chain, and Ro52/TRIM21 were measured by LIPS employing luciferase-tagged antigens as previously described (33). For the ADCC assay, NK cells were isolated from healthy subjects by immunomagnetic negative selection (EasySep Human NK Cell Isolation Kit, Stemcell Technologies) and incubated overnight with 1,000 U/ml IL-2. PBMCs from the same donor were used as targets after resting and CFSE labeling. Targets were incubated with or without NK in the presence of PBS, anti-CD20, or patient's plasma, then stained for CD3, CD4, CD8, and CD19 and analyzed by flow cytometry. Cells were enumerated using counting beads and percentage killing was calculated as the difference in the absolute number of CFSE-labeled targets incubated with and without NK. Total IgG was purified from plasma with Protein A/G agarose affinity resin (Thermo Fisher Scientific).

*Immunohistochemistry, quantitative imaging, and inflammasome analysis*. Immunohistochemical staining and quantification were performed as previously described (34, 35). Briefly, immunohistochemistry was performed on 5-μm tissue sections after heat-induced epitope retrieval followed by incubation with antibody against myxovirus resistance gene A (MxA), or collagen 1, or CD4 in combination with CD163 and

CD68. Slides were washed, blocked, and incubated with rabbit or mouse Polink-1 or -2 horseradish peroxidase and developed with Immpact DAB (3,3′-diaminobenzidine; Vector Laboratories). All slides were washed, counterstained, mounted, and scanned using the ScanScope CS System (Aperio Technologies), yielding high-resolution data from the entire tissue section. The percentage area positive for MxA, collagen 1, and $CD4^+$ T cells was quantified using CellProfiler version 3.1.5.

For the inflammasome activation analysis, cells were acquired using an Amnis ImageStreamX Mark II imaging flow cytometer and the integrated software INSPIRE (MilliporeSigma) was used for data collection. Additional information on immunohistochemistry and inflammasome analysis is in the supplemental material.

*Statistics*. Comparisons of continuous variables between different groups was performed by using nonparametric tests (Kruskal-Wallis test, Mann-Whitney *U* test). All hypothesis were 2-tailed and the criterion for statistical significance for these comparisons was set to $P \leq 0.05$; adjustment for multiplicity with Dunn's multiple-comparisons test was applied for the immunophenotypic analysis of T cell subsets and the analysis of the cytokines' plasma/serum concentration whenever more than 2 groups were compared. Spearman's rank correlation was used to measure the linear association between IL-7 serum levels and $CD4^+$ T cell counts.

Differential expression analysis was performed using the Bioconductor package DESeq2 (36). Genes were determined to be significantly differentially expressed if they passed multiple test correction using the Benjamini-Hochberg (37) adjusted *P* value of ≤0.05.

## Author contributions

AL and IS designed the study, provided clinical care to the enrolled patients, analyzed data, and wrote the manuscript. CSW, SLL, CG, HM, PDB, APD, AR, CAM, SLA, and CD conducted experiments, analyzed data, and/or acquired data. IL, JB, JL, MM, MVA, YM, CM, and SC provided clinical care to the enrolled patients. All authors reviewed and approved the manuscript prior to submission.

## Acknowledgments

This work has been supported in part by the intramural research program of the NIAID, NIH and in part with federal funds from the National Cancer Institute, NIH, under Contract No. HHSN261200800001E. The content of this publication does not necessarily reflect the views or policies of the Department of Health and Human Services, nor does mention of trade names, commercial products, or organizations imply endorsement by the US Government.

Address correspondence to: Andrea Lisco or Irini Sereti, 10 Center Drive, Building 10, Room 6D44G (A. Lisco) or Room 11B17 (I. Sereti), Bethesda, Maryland 20892. USA. Phone: 301.761.7122; Email: Andrea.lisco@nih.gov (A. Lisco). Phone: 301.496.5533; Email: Irini.Sereti@nih.gov (I. Sereti).

1. Engsig FN, et al. Long-term mortality in HIV patients virally suppressed for more than three years with incomplete CD4 recovery: a cohort study. *BMC Infect Dis*. 2010;10:318.
2. Kelley CF, et al. Incomplete peripheral $CD4^+$ cell count restoration in HIV-infected patients receiving long-term antiretroviral treatment. *Clin Infect Dis*. 2009;48(6):787–794.
3. Robbins GK, et al. Incomplete reconstitution of T cell subsets on combination antiretroviral therapy in the AIDS Clinical Trials Group protocol 384. *Clin Infect Dis*. 2009;48(3):350–361.
4. Lederman MM, et al. Immunologic failure despite suppressive antiretroviral therapy is related to activation and turnover of memory CD4 cells. *J Infect Dis*. 2011;204(8):1217–1226.
5. Shive CL, et al. Inflammatory cytokines drive $CD4^+$ T-cell cycling and impaired responsiveness to interleukin 7: implications for immune failure in HIV disease. *J Infect Dis*. 2014;210(4):619–629.
6. Zonios DI, et al. Idiopathic $CD4^+$ lymphocytopenia: natural history and prognostic factors. *Blood*. 2008;112(2):287–294.
7. Deng Z, et al. Inherited mutations in the helicase RTEL1 cause telomere dysfunction and Hoyeraal-Hreidarsson syndrome. *Proc Natl Acad Sci USA*. 2013;110(36):E3408–E3416.
8. Xie Z, Klionsky DJ. Autophagosome formation: core machinery and adaptations. *Nat Cell Biol*. 2007;9(10):1102–1109.
9. Marek-Yagel D, et al. Clinical disease among patients heterozygous for familial Mediterranean fever. *Arthritis Rheum*. 2009;60(6):1862–1866.
10. Jéru I, et al. The risk of familial Mediterranean fever in MEFV heterozygotes: a statistical approach. *PLoS One*. 2013;8(7):e68431.
11. Khare S, et al. An NLRP7-containing inflammasome mediates recognition of microbial lipopeptides in human macrophages. *Immunity*. 2012;36(3):464–476.
12. Seidel MG. Autoimmune and other cytopenias in primary immunodeficiencies: pathomechanisms, novel differential diagnoses, and treatment. *Blood*. 2014;124(15):2337–2344.
13. Henriksson G, Manthorpe R, Bredberg A. Antibodies to CD4 in primary Sjögren's syndrome. *Rheumatology (Oxford)*.

2000;39(2):142–147.
14. Yuen SJ, Rubin PA. Idiopathic orbital inflammation: distribution, clinical features, and treatment outcome. *Arch Ophthalmol*. 2003;121(4):491–499.
15. Monaghan TM, Albanese G, Kaye P, Thomas JD, Abercrombie LC, Moran GW. Orbital inflammatory complications of Crohn's disease: a rare case series. *Clin Med Insights Gastroenterol*. 2018;11:1179552218757512.
16. Garrity JA, Coleman AW, Matteson EL, Eggenberger ER, Waitzman DM. Treatment of recalcitrant idiopathic orbital inflammation (chronic orbital myositis) with infliximab. *Am J Ophthalmol*. 2004;138(6):925–930.
17. Doitsh G, et al. Cell death by pyroptosis drives CD4 T-cell depletion in HIV-1 infection. *Nature*. 2014;505(7484):509–514.
18. Muñoz-Arias I, Doitsh G, Yang Z, Sowinski S, Ruelas D, Greene WC. Blood-derived CD4 T cells naturally resist pyroptosis during abortive HIV-1 infection. *Cell Host Microbe*. 2015;18(4):463–470.
19. Negredo E, et al. Unexpected CD4 cell count decline in patients receiving didanosine and tenofovir-based regimens despite undetectable viral load. *AIDS*. 2004;18(3):459–463.
20. Puronen CE, et al. Decreased interleukin 7 responsiveness of T lymphocytes in patients with idiopathic CD4 lymphopenia. *J Infect Dis*. 2012;205(9):1382–1390.
21. Weinhold KJ, Lyerly HK, Stanley SD, Austin AA, Matthews TJ, Bolognesi DP. HIV-1 GP120-mediated immune suppression and lymphocyte destruction in the absence of viral infection. *J Immunol*. 1989;142(9):3091–3097.
22. Luo Z, et al. Pathological role of anti-CD4 antibodies in HIV-infected immunologic nonresponders receiving virus-suppressive antiretroviral therapy. *J Infect Dis*. 2017;216(1):82–91.
23. Lyerly HK, et al. Anti-GP 120 antibodies from HIV seropositive individuals mediate broadly reactive anti-HIV ADCC. *AIDS Res Hum Retroviruses*. 1987;3(4):409–422.
24. Tabb B, et al. Reduced inflammation and lymphoid tissue immunopathology in rhesus macaques receiving anti-tumor necrosis factor treatment during primary simian immunodeficiency virus infection. *J Infect Dis*. 2013;207(6):880–892.
25. Hsu DC, et al. A paradoxical treatment for a paradoxical condition: infliximab use in three cases of mycobacterial IRIS. *Clin Infect Dis*. 2016;62(2):258–261.
26. Calabrese LH, Zein N, Vassilopoulos D. Safety of antitumour necrosis factor (anti-TNF) therapy in patients with chronic viral infections: hepatitis C, hepatitis B, and HIV infection. *Ann Rheum Dis*. 2004;63 Suppl 2:ii18–ii24.
27. Habib SF, Hasan MZ, Salam I. Infliximab therapy for HIV positive Crohn's disease: A case report. *J Crohns Colitis*. 2009;3(4):302–304.
28. Beltrán B, Nos P, Bastida G, Iborra M, Hoyos M, Ponce J. Safe and effective application of anti-TNF-alpha in a patient infected with HIV and concomitant Crohn's disease. *Gut*. 2006;55(11):1670–1671.
29. Wagner CL, et al. Short telomere syndromes cause a primary T cell immunodeficiency. *J Clin Invest*. 2018;128(12):5222–5234.
30. Côté HC, et al. Leukocyte telomere length in HIV-infected and HIV-exposed uninfected children: shorter telomeres with uncontrolled HIV viremia. *PLoS One*. 2012;7(7):e39266.
31. Kim D, Langmead B, Salzberg SL. HISAT: a fast spliced aligner with low memory requirements. *Nat Methods*. 2015;12(4):357–360.
32. Stoddard JL, Niemela JE, Fleisher TA, Rosenzweig SD. Targeted NGS: a cost-effective approach to molecular diagnosis of PIDs. *Front Immunol*. 2014;5:531.
33. Burbelo PD, Lebovitz EE, Notkins AL. Luciferase immunoprecipitation systems for measuring antibodies in autoimmune and infectious diseases. *Transl Res*. 2015;165(2):325–335.
34. Schuetz A, et al. Initiation of ART during early acute HIV infection preserves mucosal Th17 function and reverses HIV-related immune activation. *PLoS Pathog*. 2014;10(12):e1004543.
35. Carpenter AE, et al. CellProfiler: image analysis software for identifying and quantifying cell phenotypes. *Genome Biol*. 2006;7(10):R100.
36. Love MI, Huber W, Anders S. Moderated estimation of fold change and dispersion for RNA-seq data with DESeq2. *Genome Biol*. 2014;15(12):550.
37. Benjamini Y, Drai D, Elmer G, Kafkafi N, Golani I. Controlling the false discovery rate in behavior genetics research. *Behav Brain Res*. 2001;125(1–2):279–284.